Tectonophysics 454 (2008) 14–22

Contents lists available at ScienceDirect

Tectonophysics

journal homepage: www.elsevier.com/locate/tecto

The structure of the lower crust at the Argentine continental margin, South Atlantic at 44°S

Michael Schnabel [a,*], Dieter Franke [a], Martin Engels [a], Karl Hinz [a], Sönke Neben [a], Volkmar Damm [a], Stefan Grassmann [b], Hugo Pelliza [c], Paulo Ricardo Dos Santos [c]

[a] Federal Institute for Geosciences and Natural Resources (BGR), Stilleweg 2, D-30655 Hannover, Germany
[b] Aabar Petroleum Investments Company PJSC, Ministry of Energy Building, Corniche Road, P.O. Box: 107888, Abu Dhabi, United Arab Emirates
[c] Petrobras Energía S.A., Maipú 1-17th Floor, C1084ABA Buenos Aires, Argentina

ARTICLE INFO

Article history:
Received 16 July 2007
Received in revised form 14 January 2008
Accepted 29 January 2008
Available online 4 March 2008

Keywords:
Volcanic passive margins
Seismic tomography
South Atlantic
Continental rifting
Magma emplacement

ABSTRACT

It is well established that the Argentine passive margin is of the rifted volcanic margin type. This classification is based primarily on the presence of a buried volcanic wedge beneath the continental slope, manifested by seismic data as a seaward dipping reflector sequence (SDRS). Here, we investigate the deep structure of the Argentine volcanic margin at 44°S over 200 km from the shelf to the deep oceanic Argentine Basin. We use wide-angle reflection/refraction seismic data to perform a joint travel time inversion for refracted and reflected travel times. The resulting P-wave velocity-depth model confirms the typical volcanic margin structure. An underplated body is resolved as distinctive high seismic velocity (v_p up to 7.5 km/s) feature in the lower crust in the prolongation of a seaward dipping reflector sequence. A remarkable result is that a second, isolated body of high seismic velocity (v_p up to 7.3 km/s) exists landward of the first high-velocity feature. The centres of both bodies are 60 km apart. The high-velocity lower-crustal bodies likely were emplaced during transient magmatic–volcanic events accompanying the late rifting and initial drifting stages. The lateral variability of the lower crust may be an expression of a multiple rifting process in the sense that the South Atlantic rift evolved by instantaneous breakup of longer continental margin segments. These segments are confined by transfer zones that acted as rift propagation barriers. A lower-crustal reflector was detected at 3 to 5 km above the modern Moho and probably represents the lower boundary of stretched continental crust. With this finding we suggest that the continent–ocean boundary is situated 70 km more seaward than in previous interpretations.

1. Introduction

The theory of plate tectonic or the earlier continental drift hypothesis (Wegener, 1912; Du Toit, 1937) was initially pushed on the geometrical fit of shelf edges and on the continuity of geological features across the continents. In particular the southern South Atlantic allowed a first mathematical reassembly accomplished by sequentially fitting pairs of continents after determining their best fitting poles of rotation (Bullard et al., 1965). Most plate-tectonic models describe the early opening of the southern South Atlantic as a more or less continuous northward propagating unzipping of rift zones (e.g., Nürnberg and Müller, 1991; Jackson et al., 2000). The southern segment of the South Atlantic (between the Walvis/Rio Grande Ridges and the Falkland–Agulhas Fracture Zone) is undisturbed from major regional jumps of the spreading axis and there are no complex oceanic features, like volcanic ridges or volcanic plateaus. As the majority of the passive margins (Skogseid, 2001; Menzies et al., 2002), the South Atlantic is of the rifted volcanic margin type. The Early Cretaceous South Atlantic continental breakup (Nürnberg and Müller, 1991) and initial seafloor spreading were accompanied by extensive transient volcanism and magmatism recorded as inferred sill intrusions, flood basalt sequences, voluminous volcanic wedges, and magmatic underplating. In seismic reflection data the voluminous extrusives are manifested by huge wedges of seaward dipping reflectors (SDRS) on both sides of the southern South Atlantic (Gladczenko et al., 1997; Hinz et al., 1999). Bauer et al. (2000) showed that the lower crust beneath the seaward dipping reflectors off Namibia shows high velocities of 7.3 km/s. This high-velocity lower crust (HVLC) is a typical feature which occurs at volcanic rifted margins between stretched continental crust and oceanic crust of normal thickness (e.g., Kelemen and Holbrook, 1995; Korenaga et al., 2000). Most likely the emplacement of the HVLC accompanied the breakup stage and was associated with mantle upwelling (e.g., Kelemen and Holbrook, 1995; Boutilier and Keen, 1999). In the case of the Namibia margin, the continent–ocean transition is rather abrupt with the HVLC occupying almost the entire crustal space and forming the western edge of a slightly thinned continental crust (Bauer et al., 2000). In this case, a rather sharp transition from continental to transitional/normal oceanic crust, the formation of a lower-crustal body may be better ascribed to relative

* Corresponding author. Tel.: +49 511 6432912; fax: +49 511 6433663.
E-mail address: Michael.Schnabel@bgr.de (M. Schnabel).

0040-1951/$ – see front matter © 2008 Elsevier B.V. All rights reserved.
doi:10.1016/j.tecto.2008.01.019

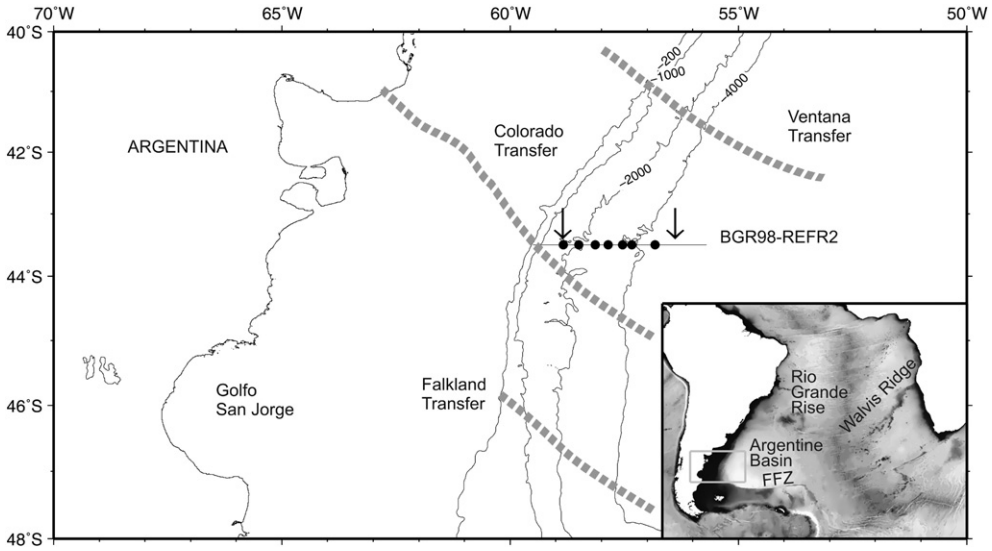

Fig. 1. The study area offshore Argentina and location of the refraction seismic line BGR98-REFR2. The positions of ocean bottom hydrophones (from OBH 2-8 at the west to OBH 2-2 at the east) are marked as black dots. Arrows show the range of the profile this paper focuses on. Thin solid lines show bathymetric contours (in meters). Transfer zones (dashed lines) after Franke et al. (2007). FFZ: Falkland–Agulhas Fracture Zone.

sharp lithospheric rupturing along the incipient plate boundary and decompressional melting rather than to plumes and/or hotspots (Menzies et al., 2002).

Prior to our experiment, no wide-angle seismic studies were carried out along the Argentine margin. Hence, the architecture of the lower crust was unknown and there was no evidence whether the well known SDRS are associated with a HVLC. Here, we present a deep seismic sounding at the Argentine continental slope. We show that the Argentine margin is a typical rifted volcanic margin with a high-velocity lower-crustal body with a width of 60 km and a thickness of 4 to 6 km beneath the seaward dipping reflector sequences (SDRS). Further we demonstrate that there is another, smaller high-velocity lower-crustal body landward of the SDRS. This structure that is well documented within the resolution of our data may be explained by multiple, interrupted rifting. A lower-crustal reflector, probably the pre-rift Moho, may be used to define the continent–ocean boundary quite precisely.

2. Geological framework

The South Atlantic is divided by the Walvis Ridge–Rio Grande Rise (Fig. 1) into two main parts. While the classification of the northern part is still ambiguous, the southern part shows all features of volcanic passive margins (e.g., Gladczenko et al., 1997; Hinz et al., 1999). In this area, the rate of initial, northward directed rifting was fast and reached values of 30 cm/year (Light et al., 1993).

All along the continental slope offshore Argentina, north of 45°S, volcanic wedges with seaward dipping reflectors (SDRS) were found (Hinz et al., 1999; Franke et al., 2007). These wedges are interpreted as basaltic flows and volcano-clastic rocks extruded near or above sea level immediate prior to and during the initial stage of normal seafloor spreading. The multi-channel seismic (MCS) section SO85-005, shown in Fig. 2 shows the typical features in the transition area from continental to oceanic crust. The shallow shelf area in the western-most part is characterised by narrow half-grabens which are filled with subparallel bedded sediments. At the slope, between 120 and 130 km, the magnetic anomaly G is located (Rabinowitz and LaBrecque, 1979). These authors proposed that this anomaly marks the continent–ocean boundary. Between 130 and 180 km, seaward dipping reflector wedges are distinct. These are subdivided into two distinct wedges, separated by a strong unconformity (Neben et al., 2005). In the eastern part the profile shows a smooth and flat lying reflection from the top of the oceanic crust. The first clearly identified magnetic anomaly M4

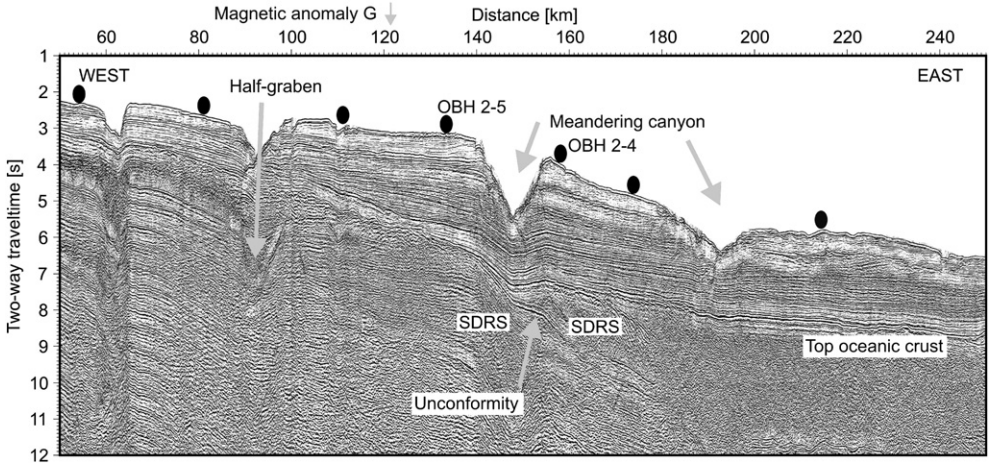

Fig. 2. Seismic section (SO85-005), which crosses the Ameghino submarine canyon and runs along the refraction seismic line (BGR98-REFR2). The distance relates to the western end of the refraction line. In the area between 130 and 180 km, the crust is characterised by two sequences of seaward dipping reflectors (SDRS), separated by a strong unconformity. Magnetic anomaly G after Rabinowitz and LaBrecque (1979).

(Rabinowitz and LaBrecque, 1979) is situated at around 160 km seaward of the feather edge of the SDRS.

3. Wide-angle seismic data

The data used in this study were acquired by the BGR during cruise BGR98 with R/V Akademik Lazarev. The wide-angle seismic profile BGR98-REFR2 (Fig. 1) runs in East–West direction at 44°S across the continental slope off Argentina along the same track as MCS line SO85-005 (Fig. 2). The water depth along this profile ranges between 1600 m and 4900 m.

The data were recorded at seven ocean bottom hydrophones (OBH), which were deployed with an average spacing of 25 km. As seismic source, an array consisting of 32 BOLT 1900 LL-X airguns with a total volume of 4258 cubic inch (69.8 l) was used. The profile was run twice with a mean shot interval of about 175 m. Stacking of both profiles improved the signal-to-noise ratio, especially at far offsets.

The refracted wave from the crust (P_g) is clearly observed at all stations. It was possible to determine 2233 travel times for this phase. 1451 reflections from the crust–mantle boundary (P_mP) were also observed along the whole profile. On the seaward half of this profile (station 2-6, 2-5 and 2-2), additional reflections (P_iP) with travel times ranging between P_g and P_mP are distinct. Example seismic sections from stations OBH 2-5 and OBH 2-4 are shown in Fig. 3.

4. Methodology and results

Since the crustal refraction (P_g) does not cover the area of the lower crust, we apply a tomography using both P_g-phases and wide-angle reflections from the crust–mantle-boundary (P_mP). The benefits of this kind of joint inversion have been proven by many recent studies (e.g., Zelt et al., 2003; Majdanski et al., 2006). The results give insights into the structure of both, the upper and the lower crust and allow us to define the spatial distribution of the underplated and intruded magmatic material.

4.1. Travel time tomography

We calculate a two-dimensional velocity-depth model by using a joint refraction and reflection travel time inversion as described by Korenaga et al. (2000). Based on the travel times of first arrivals and reflected waves, this method calculates a velocity field and the position of the reflection horizon. The velocity model is parameterised as a sheared mesh hanging beneath the seafloor. Bilinear interpolation within each parallelogram-shaped grid cell leads to a continuous velocity field. Compared to a rectangular velocity grid, the sheared mesh representation allows accurate travel time calculations even in the presence of large topographic variations. A floating reflector horizon is represented as an independent array of linear segments, where only the vertical position of each reflector node will be changed during inversion. The first step of the forward ray-tracing for both reflected and refracted phases is solved by the graph method (Moser, 1991), which is also known as the shortest path method. Since the graph method tends to over-estimate the travel times, the ray-bending method (Moser et al., 1992) was used to refine the solution.

During the inverse step, we try to estimate the perturbations of the velocity field based on the travel time residuals. For the given resolving power of typical source–receiver-geometries, the chosen fine model parameterisation (where the number of model parameters exceeds the number of observed travel times by a factor of 10) prohibits simple inversion because of strong singularity. Therefore, a regularisation is needed to stabilise the inversion. This is done by the application of smoothing constraints with pre-defined correlation lengths on both velocity and depth perturbations. To avoid any instability due to large travel time residuals, an additional damping is applied on the velocity and depth nodes (Korenaga et al., 2000).

4.2. Compilation of the starting model

We use the multi-channel seismic data of BGR's line SO85-005 (Fig. 2) to obtain information about the sedimentary cover along the profile. Based on the MCS records, the sedimentary cover can be divided into three units: the lower-most has a thickness between 1200 and 1500 m. Its top is marked by an unconformity, tentatively interpreted by Hinz et al. (1999) as Late Aptian (AR2). Interval velocities derived from stacking velocities have values ranging from 2800 m/s in the eastern part of the line to 3400 m/s in the western, landward part of the profile where its thickness almost doubles.

The top of the overlying sedimentary unit, presumably consisting of an equivalent of the Colorado Formation of the Colorado Basin

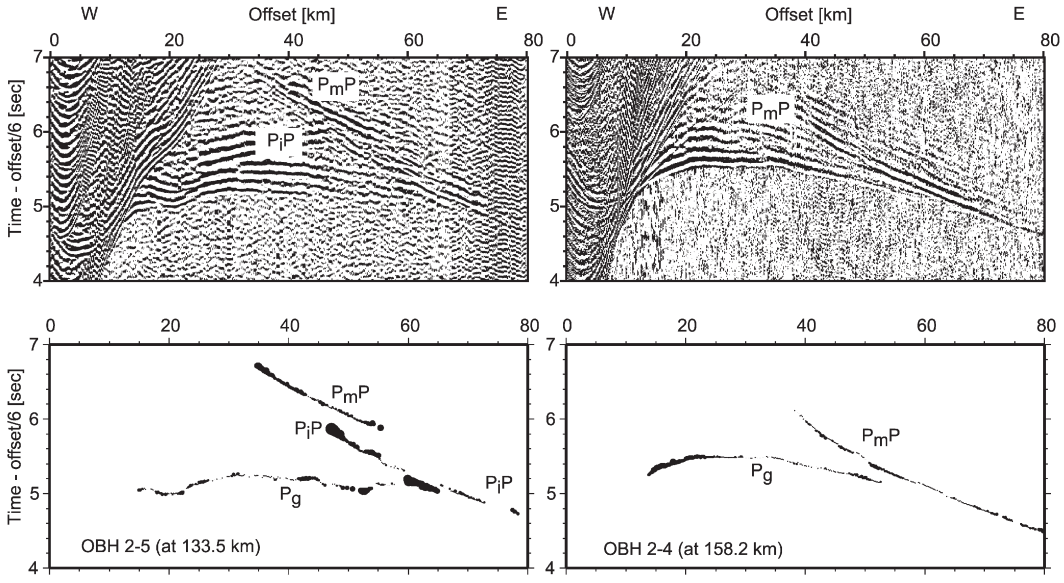

Fig. 3. Seismic sections from OBH 2-5 and OBH 2-4 (travel times are displayed with a reduction velocity of 6 km/s). The lower panels represent the travel times for the final model, were the size of the dots corresponds to the difference between picked and calculated times. The left example shows two distinct reflections (P_mP and P_iP), while the P_iP-phase cannot be observed at the more seaward station 2-4.

(Bushnell et al., 2000), is correlated with the base of the Paleocene Pedro Luro Formation (Keeley and Light, 1993). The unit shows a thickness ranging from 800 m to 1800 m, and seismic interval velocities between 2200 and 2600 m/s.

Strong sediment supply and complex depositional and erosional processes have contributed to the formation of the upper-most sedimentary unit that shows overlapping sedimentary drift structures formed by deep-water contour currents, but also gravitational sliding and canyons. The upper-most unit of primarily Neogene age (Hinz et al., 1999; Franke et al., 2007) has a thickness of up to 1000 m and velocities between 1600 and 1800 m/s.

To find a starting model for the crust, we conduct several preliminary tests using a 1-D structure. These tests are described in Section 5. Based on these results, we started with a simple model where the continental Moho is at a constant depth of 22 km. Seaward of the area of the SDRS, the crust thins linearly to a depth of 14 km (which corresponds to a crustal thickness of 6 km). The velocity of the crust ranges in the starting model linearly from 5.0 km/s at the top to 7.0 km/s at the bottom.

4.3. Travel time inversion

The model is 310 km long and has a depth of 34 km below seafloor. The horizontal grid spacing is ~1 km on average whereas vertical grid spacing is 0.1 km. The Moho reflection (the crust–mantle-boundary) was sampled at an interval of 5 km, which results in 63 depth nodes. After several tests on model regularisation, we decide to use horizontal correlation lengths ranging from 8 km at the top to 20 km at the bottom of the model. The vertical correlation length varied between 0.5 km below the seafloor and 3 km at the maximum depth of 34 km. The depth kernel weighting factor was fixed to $w=1$. With this value, velocity and depth nodes are equally weighted during the inversion of reflected phases. The RMS misfit for P_mP phases was 95 ms after 10 iterations, and after 25 iterations, the final RMS misfit was 37 ms for P_g and 69 ms for P_mP. These values correspond to χ^2 of 0.535 for refracted waves and 1.912 for reflected waves. Examples for the misfit between inverted and observed travel times are shown in Fig. 3. To explain the travel times from the P_iP phases (internal lower-crustal reflector) we introduce a floating intra-crustal reflection horizon in the final model. The resulting RMS misfit for these P_iP phases was 56 ms. For this inversion, only reflected travel times were taken into account. Therefore, there is no impedance contrast resolved at this boundary.

4.4. Resulting model

The given ray coverage define the seismic velocities between 50 and 250 km of the profile. We will focus our following discussion on this central part (Fig. 4). The profile shows the typical image of a rifted volcanic margin. The crust thins from more than 20 km at the western part of the profile to about 6 km at the eastern end. The upper crustal velocities range mainly between 4.8 km/s and 5.0 km/s. The only exception is in the area of the half-grabens (distance: 90–110 km), where the seismic velocities are in the range of 4.6 km/s. At the transition from continental to oceanic crust, i.e. at the location of the SDRS, a high-velocity lower crust (HVLC) was identified. The layer with high seismic velocity (v_p>7.0 km/s) is characterised by two distinct maxima: at 145 km it reaches a thickness of 4.5 km, while at 200 km this layer is as thick as 6.5 km. Following the 7.3 km/s isoline, the landward part (HVLC1; Fig. 4) is about 30 km wide and situated between 125 and 155 km of the profile. The seaward area (HVLC2) ranges from 180 to 220 km of the profile. Here, the seismic velocity exceeds 7.5 km/s. The inversion of the phases from a lower-crustal reflector (P_iP phases) resulted in a horizon at about 2 to 3 km above the Moho. This reflector is not observed above HVLC1.

4.5. Gravity modelling

In order to verify the crustal structure derived by travel time inversion, we perform 2D gravity modelling. For the density-depth model, strict structural constraints are given by the seafloor, sedimentary layers and the Moho. These boundaries were kept fixed throughout modelling. Further constraints are the location of SDRS known from MCS and the geometry of the HVLC as resolved by the seismic tomography.

In Fig. 5, the resulting gravity model is shown in combination with the final velocity model. Densities of model blocks represent a mean value following the velocity-density conversion law by Ludwig et al.

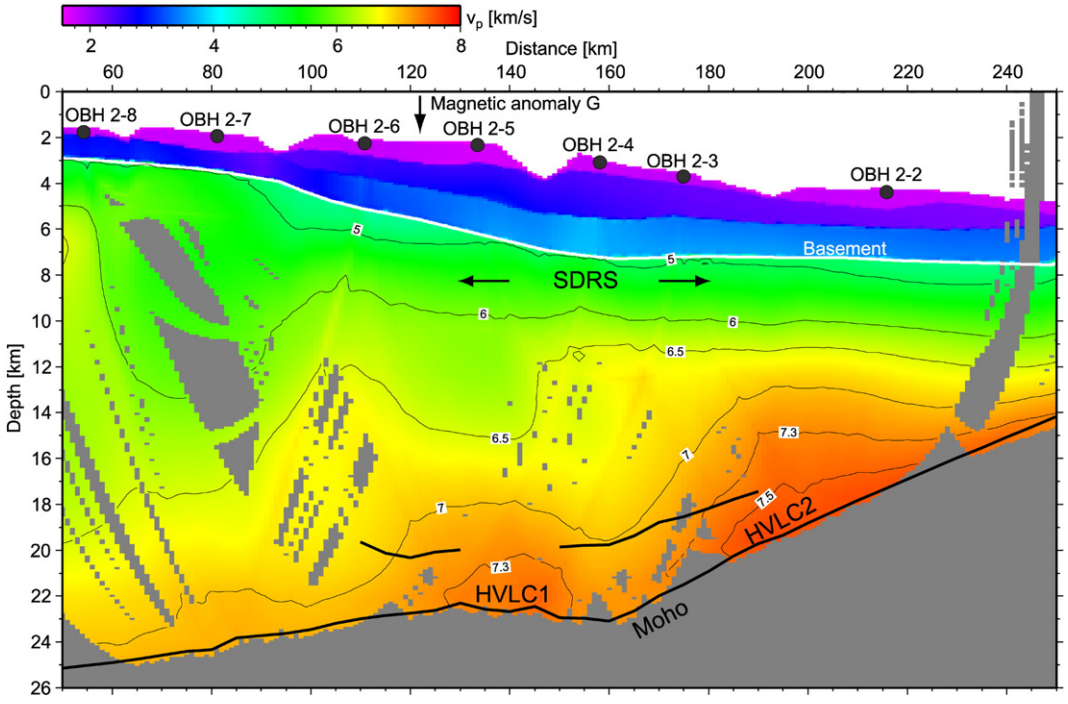

Fig. 4. The resulting velocity-depth distribution along the profile BGR98-REFR2 (same area as shown in Fig. 2).

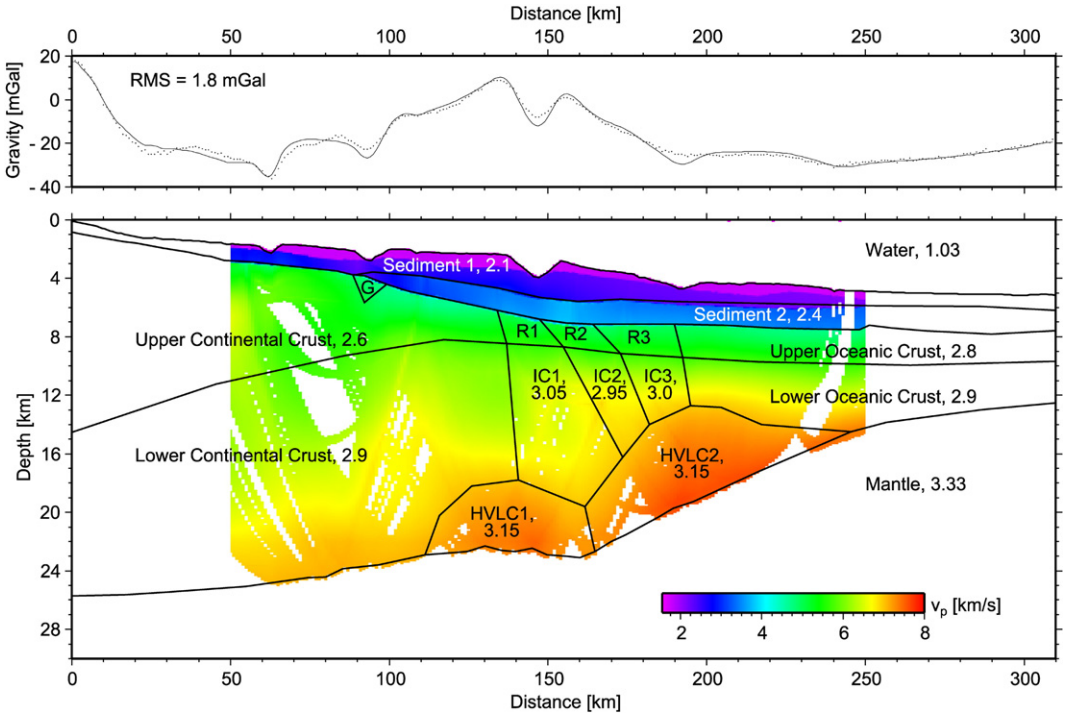

Fig. 5. Result of the gravity modelling. The line drawing shows the different blocks and their density. R1: SDR sequence 1 (density=2.85 g/cm^3), R2: SDR sequence 2 (2.80 g/cm^3), R3: SDR sequence 3 (2.80 g/cm^3), G: half-graben (2.80 g/cm^3), IC: intruded crust. The upper panel shows the model response (solid line) and the measured free-air gravity (points).

(1970). The gravity model extends beyond the tomography profile to a normal continental and oceanic crustal model, respectively.

The upper panel of Fig. 5 displays the model response fitting the observed marine free-air gravity data reasonably (RMS error of 1.8 mGal). The edge of the HVLC with a density of 3.15 g/cm^3 coincides with the P-wave velocity isoline of 7.0 km/s. Densities of the SDRS correspond to upper oceanic crust (2.8 g/cm^3), with the presumably oldest dipping reflector sequence (R1 in Fig. 5) being slightly denser (2.85 g/cm^3).

Various modelling attempts showed that SDRS and HVLC alone cannot explain the gravity data. The results would be either unrealistic high densities or a mass deficit of the crust in between. Reasonable densities in the area below the SDRS range from 2.95 to 3.05 g/cm^3. These values exceed the normal lower-crustal density of 2.9 g/cm^3 and may be interpreted as heavily intruded crust.

The crustal area below the SDRS is the only part in the model where we could not use the velocity–density conversion law as derived by Ludwig et al. (1970). However, Korenaga et al. (2001) described a similar phenomenon for the southeast Greenland margin. Their plausible interpretation of the gravity anomaly is a denser upper crust in the continent–ocean transition zone, utilising a different velocity–density conversion law for mafic rocks (e.g., Planke 1994) which allows densities around 3.0 g/cm^3 for P-wave velocities of 6.5 km/s. Korenaga et al. (2001) explain these different conversion laws by their sensitivity to the porosity structure (pore aspect ratio).

We conclude the seismic tomography result resolving underplated bodies is confirmed by gravity data without modifying any structural boundaries, if the conversion law of mafic rocks applies to the heavily intruded crust above. Keeping limitations of 2D-modelling in mind, a local gravity high south of our profile at 44°S might indicate a minor long wavelength contribution to the gravity high, a target for future 3D gravity modelling.

5. Sensitivity tests and model constrains

The spatial distribution of rays in our final model is shown in Fig. 6. The sedimentary layer and the upper crust is well covered by refracted waves down to a depth of 10 to 12 km. Fig. 6c shows that the crust–mantle boundary is imaged by reflected waves for nearly the whole profile. A more concise measure for the ray coverage is the derivative weight sum (DWS), which is the column-sum vector of the Fréchet

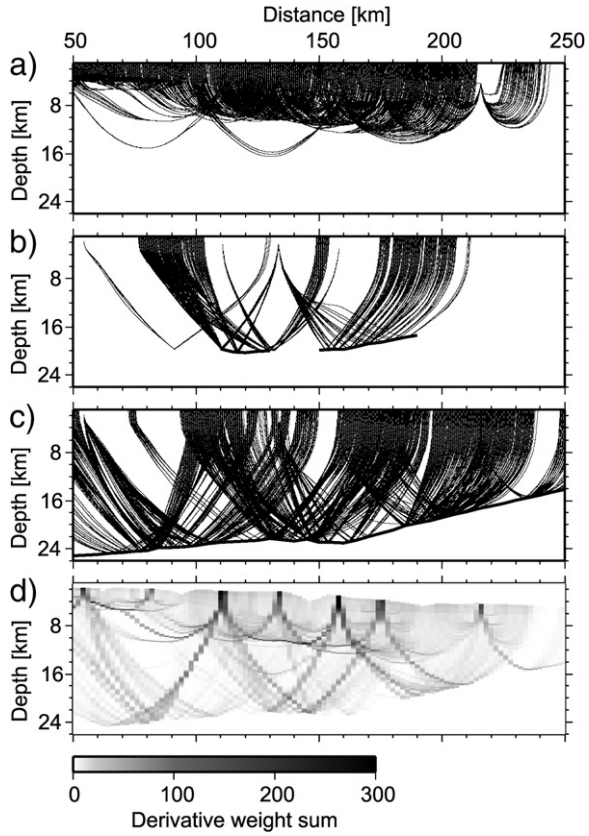

Fig. 6. Ray coverage for refracted phases (a), reflections from the intra-crustal discontinuity (b), and for reflections from the crust–mantle-boundary (c). Fig. 5d shows the values of the derivative weight sum.

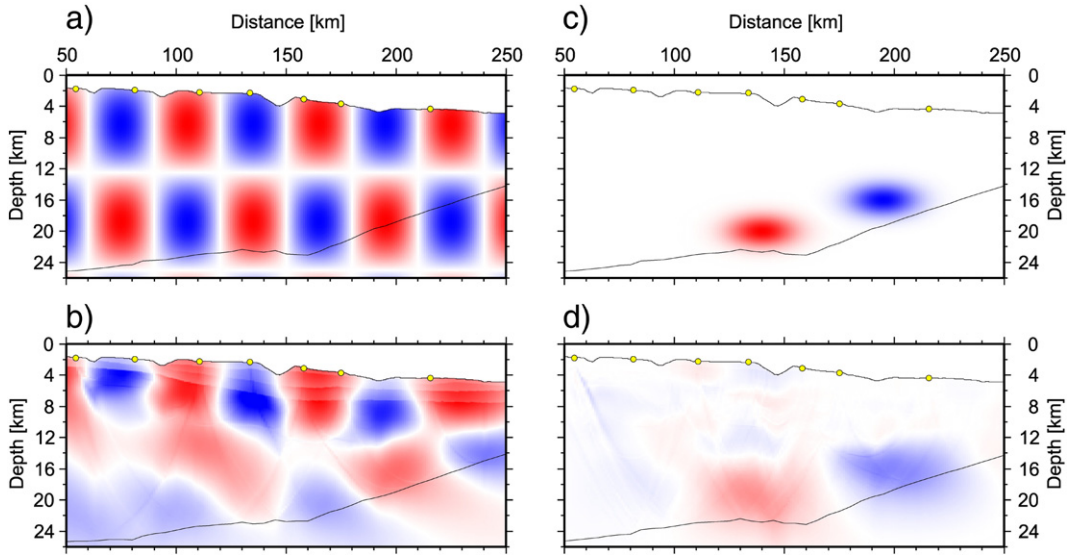

Fig. 7. Results of the checkerboard tests. The upper panels show the velocity perturbations which were applied to the resulting model (Fig. 4). The lower panels show the recoveries after 8 iterations.

velocity kernel (Toomey and Foulger, 1989). The DWS is a measure for the linear sensitivity of the inversion and is presented in Fig. 6d.

The question rises whether the distinct separation of the high-velocity lower crust (HVLC) is within the resolution of our data. To investigate the capability of the tomography to map small structures within the crust we perform a checkerboard test. The final model of Fig. 4 was perturbed by velocity variations ±5% within cells that had a dimension of 12.5×30 km (Fig. 7a). Based on this perturbed model, we calculate synthetic travel times using the given source–receiver geometry. After adding a random noise of 50 ms, these synthetic travel times are used as input for another tomographic inversion, where the final model of Fig. 4 is used as input model. The result (Fig. 7b) shows that these artificial velocity perturbations are well resolved in the area of the two high-velocity lower-crustal bodies. We conduct a second resolution test, where we focus on the lower crust (Fig. 7c). The perturbations have the spatial dimensions of the separate areas of HVLC. The obtained recovery is shown in Fig. 7d. Based on these results, we argue that our data set has enough resolving power to image the two separated areas of the HVLC.

Another argument against the spatially separated high-velocity lower-crustal bodies may be the ambiguity between the depth level of the Moho and velocity variations within the lower crust. To test this velocity-depth ambiguity, Korenaga et al. (2000) suggested exploring the solution space systematically by changing the value of the depth kernel weighting parameter w, which controls the relative weighting of velocity and depth parameters during the P_mP inversion. We repeat the inversion with $w=0.01$ (which allows more velocity perturbations than depth perturbations) and $w=100$ (where the variations of the reflector are allowed to be larger). In both cases, the reflector is imaged at nearly the same depth (Fig. 8). The 7 km/s isoline clearly shows the separation of the two areas of the HVLC and confirms the reliability of the lower-crustal velocities.

Finally we want to explore possible bias resulting from the starting model. To obtain a reliable starting model for the crustal part of our profile and to investigate the sensitivity of the final model on the starting model, we conduct a Monte Carlo test. The input were ten velocity models with varying seismic velocities at the top of the crust between 4.4 and 5.2 km/s and two different velocity-depth-gradients but with no lateral variation within the crust. We combine each of these models with one of ten different reflectors (horizontal) at a depth between 15 and 24 km. This resulted in 100 different starting models. For each of these models, we calculate a travel time tomography as described in Section 4.3. The mean value of all results is shown in Fig. 9. A striking result is the shape of the resulting reflector. The average reflector is more or less horizontal in the western part of the profile, while it shallows linearly seaward of profile km 160 of the profile. All resulting reflectors show no more than 1000 m deviation from the average reflector. The resulting

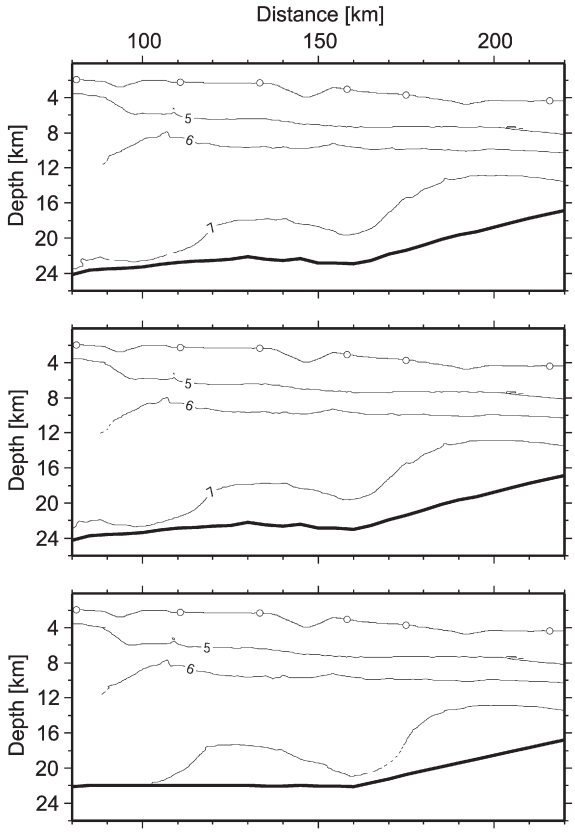

Fig. 8. Results of the depth kernel (w) weighting test. The resulting velocity-isolines and the position of the reflector are shown for $w=100$ (top), $w=1$ (middle, same as Fig. 4) and $w=0.01$ (bottom). All inversions deliver similar result.

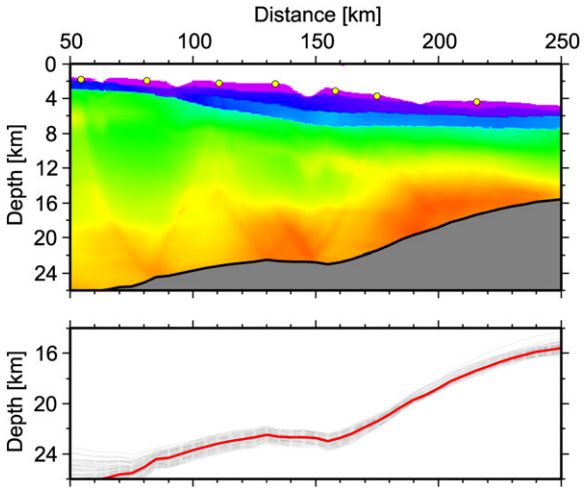

Fig. 9. Results of the Monte Carlo test. The lower box shows the resulting reflectors for all 100 starting models (grey lines), while the average reflector is shown in red. The upper box represents the average velocity model and the average reflector.

average velocity model also confirms the separation of the HVLC into two parts. Therefore, we argue that the results we described in detail in Section 4.4 do not depend on the starting model.

6. Discussion

6.1. Structure and emplacement

We show that the volcanic continental margin offshore Argentina at 44°S is characterised by the existence of a lower-crustal body with seismic velocities exceeding 7.0 km/s. The 7.3 km/s isoline shows that this area is divided into two separate units. One high-velocity body (HVLC2) is centred beneath the seaward end of the SDRS and another one (HVLC1) some 60 km landward of these (Fig. 10). The latter underlies stretched continental crust with a thickness of 14 km and might be interpreted as an intrusion. Bauer et al. (2000) found intrusions of similar size landward of the main underplated body off Namibia. However, in contrast to the structure identified at the Namibian margin, the continentward located velocity variation at the Argentine margin is limited to the deepest 5 km of the lower crust and extends some 30 km horizontally. We suggest that this shape is more likely the expression of underplating rather than an intrusion. If the landward body (HVLC1) was formed by an intrusion we have had no problem with the timing. Twofold underplating, however implies multiple discrete steps of rifting and probably adiabatic decompressional melt generation. A mantle plume as source for the two HVLC bodies could explain the structures only by assuming discrete pulses that should be observable over a wider area. The location of the refraction seismic line close to a transfer zone (Colorado Transfer zone; Max et al., 1999; Franke et al., 2007) however may give a reasonable explanation for this temporal variability of magmatic processes. The idea behind this hypothesis is that the oceanic basin evolved by instantaneous breakup of longer sections rather than by continuous propagating rifting. The transfer zones act as rift propagation barriers in this theory. Deep and relatively sharp lithosphere rupturing in form of fast propagating rift zones have been inferred as mechanism for transient excess melting by decompression for the diachronous emplacement of the SDRS along the Argentine margin (Hinz et al., 1999). If the assumption of interrupted rifting is correct heat accumulation is likely to occur, resulting in enhanced convection in the asthenosphere (e.g. Mutter et al., 1988; Saunders et al., 1997) and subsequently magmatic underplating.

Spatially separated HVLC were previously detected by Mjelde et al. (2003). These authors analysed wide-angle seismic models from the Vøring Margin, North Atlantic. They found a strong variability in the thickness of the lower-crustal high-velocity layer and suggested three separated injection centres within the upper mantle as reason for this variability. Further, they noted that the distribution of the lower-crustal bodies is linked to pre-rift crustal lineaments.

Another result of our study is the existence of a lower-crustal reflector that was unequivocally verified in the centre of the profile (Fig. 4). It is interrupted above HVLC1 and its eastern end is situated above the centre of HVLC2. Our best guess is that this reflector represents the former Moho discontinuity of the stretched continental crust before the onset of magmatic underplating. At a depth of 18–20 km the interpretation of this reflector as Conrad discontinuity is unlikely. Alternatively, it may be interpreted as a brittle–ductile transition that evolved during the main phase of crustal extension. However, we resolved velocities higher than 7.0 km/s beneath this reflector which are very uncommon for (stretched) continental crust. Therefore, we suggest that the reflector marks the lower boundary of the stretched continental crust, disturbed or disrupted by the magmatic underplating. With this finding we may define the limit of the continental crust more precisely than earlier. The continental crust extends in this interpretation for 70 km seaward of the prominent magnetic anomaly G, which is often referred to as the continent–ocean boundary. Based on our model, we propose that the continent–ocean boundary is situated at around km 190 of the profile, which correlates to the seaward limit of the SDRS.

6.2. Implications

Although there may be variations in extent and thickness of the HVLC, it probably exists along the whole Argentine margin that is characterised

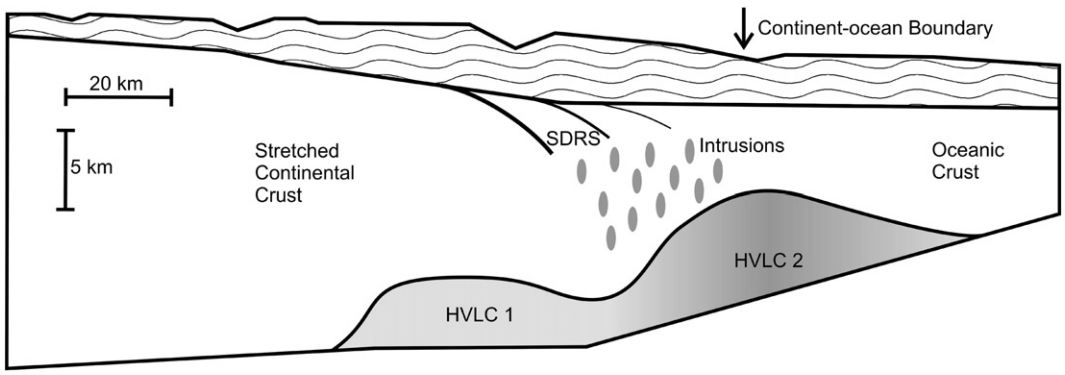

Fig. 10. Schematic interpretation of the profile. In the prolongation of the seaward dipping reflector sequences (SDRS), the second area of high-velocity lower crust (HVLC2) is situated. The landward area of high-velocity lower crust (HVLC1) shows a slightly lower velocity and is situated below stretched continental crust.

by SDRS. This underplated body has important implications for the thermal history of the early breakup and the post-rift subsidence. Fjeldskaar et al. (2003) have shown that the emplacement of a similar magmatic body below the Gjallar Ridge (Norway) has caused a short-lived increase in heat flow by up to 100 mW/m^2. Sclater et al. (1980) calculated heat flow values between 20 and 200 mW/m^2 following the first 20 m.y. of opening of the South Atlantic. With the existence of a lower-crustal body, we suggest that initial heat flow values shortly after continental rifting would lie in the upper half of this proposed range.

Regarding the subsidence we propose on the base of North Atlantic studies (e.g. Skogseid, 2001) that it was reduced in the range between 0.8 and 1.5 km due to the underplated magmatic body of a thickness of 3 to 5 km.

The crust is heavily stretched. In the western part of the model it shows a thickness of 22 km while it is only 14 km at the eastern end of the SDRS. This would give a stretching value (β) of 1.6. This value represents a minimum, as the profile probably did not reach unstretched crust at the western end. Deep seismic soundings in the Colorado Basin on the Argentine shelf revealed a crustal thickness of about 30 km (Franke et al., 2006). With this value we would obtain a β value of 2.1. It is worth noting, that the narrow half-grabens beneath the slope are much too small to account for such an amount of crustal thinning, implying that depth-dependent lithospheric stretching (e.g. Davis and Kusznier, 2004) played a major role in the formation of the southern South Atlantic.

Based on the results of our tomographic inversion, we attempt a model for the evolution of the crust in this area of the South Atlantic. During the first stage of rifting, crustal thinning resulted probably in passive upwelling of the asthenosphere and melt generation by adiabatic decompression (Furlong and Fountain, 1986). This mechanism of melt generation is further enhanced by the onset of small scale convection (Mutter et al., 1988). Due to the density contrast between the old crust and the new melt (Eldholm et al., 1995), magma accumulated at the base of the already thinned continental crust. The lower boundary of the stretched crust corresponds with the lower-crustal reflector, which is imaged at a depth between 18 and 20 km. We consider such a magma-accumulation below the crust as possible explanation for the landward high-velocity lower crust (HVLC1). Analogue models for this kind of magma emplacement are presented by Bonini et al. (2001).

During a second step of rifting, which started from the Colorado Transfer and propagated to the north, the continental crust was ruptured in the area of our deep seismic profile. During this stage the emplacement of the SDRS complexes took place coinciding with the formation of the second HVLC body at 180 to 220 km. This kind of spatial relationship between SDRS and HVLC is well known from passive volcanic margins as e.g. the North Atlantic (Eldholm and Grue, 1994).

Acknowledgements

This work was funded by Petrobras Energía S.A. and BGR as part of a joint research project of Petrobras Energía S.A. and the Federal Institute for Geosciences and Natural Resources (BGR). We gratefully acknowledge the support given by Petrobras Energía S.A.. The manuscript benefited from instructive reviews of Thomas Funck and an anonymous reviewer.

References

Bauer, K., Neben, S., Schreckenberger, B., Emmermann, R., Hinz, K., Fechner, N., Gohl, K., Schulze, A., Trumbull, R.B., Weber, K., 2000. Deep structure of the Namibia continental margin as derived from integrated geophysical studies. J. Geophys. Res. 105, 25829–25853. doi:10.1029/2000JB900227.

Bonini, M., Sokoutis, D., Mulugeta, G., Boccaletti, M., Corti, G., Innocenti, F., Manetti, P., Mazzarini, F., 2001. Dynamics of magma emplacement in centrifuge models of continental extension with implications for flank volcanism. Tectonics 20, 1053–1065. doi:10.1029/2001TC900017.

Boutilier, R.R., Keen, C.E., 1999. Small-scale convection and divergent plate boundaries. J. Geophys. Res. 104, 7389–7403. doi:10.1029/1998JB900076.

Bullard, E., Everett, J.E., Smith, A.G., 1965. The fit of continents around the Atlantic. Philos. Trans. R. Soc. Lond. 258A, 41–51.

Bushnell, D.C., Baldi, J.E., Bettini, F.H., Franzin, H., Kovas, E., Marinelli, R., Wartenburg, G.J., 2000. Petroleum system analysis of the Eastern Colorado Basin, offshore northern Argentina. In: Mello, M.R. (Ed.), Petroleum Systems of South Atlantic Margins. Am. Assoc. Petrol. Geol. Mem., vol. 29, pp. 403–415.

Davis, M., Kusznier, N., 2004. Depth-dependent lithospheric stretching at rifted continental margins. In: Karner, G.D., Taylor, B., Driscoll, N.W., Kohlstedt, D.L. (Eds.), Rheology and Deformation of the Lithosphere at Continental Margins. MARGINS Theoretical and Experimental Earth Sciences Series. Columbia University Press, pp. 92–137.

Du Toit, A.L., 1937. Our Wandering Continents; An Hypothesis of Continental Drifting. Oliver and Boyd, Edinburgh.

Eldholm, O., Grue, K., 1994. North Atlantic volcanic margins: dimensions and production rates. J. Geophys. Res. 99, 2955–2968. doi:10.1029/93JB02879.

Eldholm, O., Skogseid, J., Planke, S., Gladczenko, T.P., 1995. Volcanic margin concepts. In: Banda, E., Torné, M., Talwani, M. (Eds.), Rifted Ocean–Continent Boundaries. Kluwer Academic Publishers, pp. 1–16.

Fjeldskaar, W., Johansen, H., Dodd, T.A., Thompson, M., 2003. Temperature and maturity effects of magmatic underplating in the Gjallar Ridge, Norwegian Sea. In: Düppenbecker, S., Marzi, R. (Eds.), Multidimensional Basin Modeling. AAPG/Datapages Discovery Series, vol. 7, pp. 71–85.

Franke, D., Neben, S., Schreckenberger, S., Schulze, A., Stiller, M., Krawczyk, C.M., 2006. Crustal structure across the Colorado Basin, offshore Argentina. Geophys. J. Int. 165, 850–864. doi:10.1111/j.1365-246X.2006.02907.x.

Franke, D., Neben, S., Ladage, S., Schreckenberger, B., Hinz, K., 2007. Margin segmentation and volcano-tectonic architecture along the volcanic margin off Argentina/Uruguay, South Atlantic. Mar. Geol. 244, 46–67. doi:10.1016/j.margeo.2007.06.009.

Furlong, K.P., Fountain, D.M., 1986. Continental crustal underplating: thermal considerations and seismic–petrologic consequences. J. Geophys. Res. 91, 8285–8294.

Gladczenko, T.P., Hinz, K., Eldholm, O., Meyer, H., Neben, S., Skogseid, J., 1997. South Atlantic volcanic margins. J. Geol. Soc. (Lond.) 154, 465–470.

Hinz, K., Neben, S., Schreckenberger, B., Roeser, H.A., Block, M., Goncalves de Souza, K., Meyer, H., 1999. The Argentine margin north of 48°S: sedimentary successions, volcanic activity during breakup. Mar. Pet. Geol. 16, 1–25. doi:10.1016/S0264-8172(98)00060-9.

Jackson, M.P.A., Cramez, C., Fonck, J.-M., 2000. Role of subaerial volcanic rocks and mantle plumes in creation of South Atlantic margins: implications for salt tectonics and source rocks. Mar. Pet. Geol. 17, 477–498. doi:10.1016/S0264-8172(00)00006-4.

Korenaga, J., Holbrook, W.S., Kent, G.M., Kelemen, P.B., Detrick, R.S., Larsen, H.-C., Hopper, J.R., Dahl-Jensen, T., 2000. Crustal structure of the southeast Greenland margin from joint refraction and reflection seismic tomography. J. Geophys. Res. 105, 21591–21614. doi:10.1029/2000JB900188.

Korenaga, J., Holbrook, W.S., Detrick, R.S., Kelemen, P.B., 2001. Gravity anomalies and crustal structure at the southeast Greenland margin. J. Geophys. Res. 106, 8853–8870. doi:10.1029/2000JB900416.

Keeley, M.L., Light, M.P.R., 1993. Basin evolution and prospectivity of the Argentine continental margin. J. Pet. Geol. 16, 451–464.

Kelemen, P.B., Holbrook, W.S., 1995. Origin of thick, high-velocity igneous crust along the U.S. East Coast Margin. J. Geophys. Res. 100, 10077–10094. doi:10.1029/95JB00924.

Light, M.P.R., Keeley, M.L., Maslanyi, M.P., Urien, C.M., 1993. The tectono-stratigraphic development of Patagonia, and its relevance to hydrocarbon exploration. J. Pet. Geol. 16, 465–482.

Ludwig, W.J., Nafe, J.E., Drake, C.L., 1970. Seismic refraction. In: Maxwell, A.E. (Ed.), The Sea, vol. 4. Wiley-Interscience, pp. 53–84 (part 1).

Majdanski, M., Grad, M., Guterch, A., SUDETES 2003 Working Group, 2006. 2-D seismic tomographic and ray tracing modelling of the crustal structure across the Sudetes Mountains basing on SUDETES 2003 experiment data. Tectonophysics 413, 249–269. doi:10.1016/j.tecto.2005.10.042.

Max, M.D., Ghidella, M., Kovacs, L., Paterlini, M., Valladares, J.A., 1999. Geology of the Argentine continental shelf and margin from aeromagnetic survey. Mar. Pet. Geol. 16, 41–64. doi:10.1016/S0264-8172(98)00063-4.

Menzies, M.A., Klemperer, S.L., Ebinger, C.J., Baker, J., 2002. Characteristics of volcanic rifted margins. In: Menzies, M.A., Klemperer, S.L., Ebinger, C.J., Baker, J. (Eds.), Volcanic Rifted Margins. Geological Society of America Special Paper, vol. 362, pp. 1–14.

Mjelde, R., Shimamura, H., Kanazawa, T., Kodaira, S., Raum, T., Shiobara, H., 2003. Crustal lineaments, distribution of lower crustal intrusives and structural evolution of the Vøring Margin, NE Atlantic; new insight from wide-angle seismic models. Tectonophysics 369, 199–218. doi:10.1016/S0040-1951(03)00199-9.

Moser, T.J., 1991. Shortest path calculation of seismic rays. Geophysics 56, 59–67. doi:10.1190/1.1442958.

Moser, T.J., Nolet, G., Snieder, R., 1992. Ray bending revisited. Bull. Seismol. Soc. Am. 82, 259–288.

Mutter, J.C., Buck, W.R., Zehnder, C.M., 1988. Convective partial melting 1. A model for the formation of thick basaltic sequences during the initiation of spreading. J. Geophys. Res. 93, 1031–1048. doi:10.1029/88JB01255.

Neben, S., Franke, D., Schreckenberger, B., Temmler, T., 2005. The conjugate volcanic continental margins of the South Atlantic. Eos Trans. AGU 86 (52) Fall Meet. Suppl., Abstract T43B-1402.

Nürnberg, D., Müller, R.D., 1991. The tectonic evolution of the South Atlantic from Late Jurassic to present. Tectonophysics 191, 27–53. doi:10.1016/0040-1951(91)90231-G.

Planke, S., 1994. Geophysical response of flood basalts from analysis of wire line logs: Ocean Drilling Program Site 642, Vøring volcanic margin. J. Geophys. Res. 99, 9279–9296. doi:10.1029/94JB00496.

Rabinowitz, P.D., LaBrecque, J., 1979. The Mesozoic South Atlantic Ocean and evolution of its continental margins. J. Geophys. Res. 84, 5973–6002.

Saunders, A.D., Fitton, J.G., Kerr, A.C., Norry, M.J., Kent, R.W., 1997. The North Atlantic igneous province. In: Mahoney, J., Coffin, M.F. (Eds.), Large Igneous Provinces: Continental, Oceanic, and Planetary Flood Volcanism. AGU geophysical monograph, pp. 45–93.

Sclater, J.G., Jaupart, C., Galson, D., 1980. The heat flow through oceanic and continental crust and the heat loss of the earth. Rev. Geophys. Space Phys. 18, 269–311.

Skogseid, J., 2001. Volcanic margins: geodynamic and exploration aspects. Mar. Pet. Geol. 18, 457–461. doi:10.1016/S0264-8172(00)00070-2.

Toomey, D.R., Foulger, G.R., 1989. Tomographic inversion of local earthquake data from the Hengrill–Grensdalur central volcano complex, Iceland. J. Geophys. Res. 94, 17497–17510. doi:10.1029/89JB01087.

Wegener, A., 1912. Die Entstehung der Kontinente. Geol. Rundsch. 3, 276–292.

Zelt, C.A., Sain, K., Naumenko, J.V., Sawyer, D.S., 2003. Assessment of crustal velocity models using seismic refraction and reflection tomography. Geophys. J. Int. 153, 609–626. doi:10.1046/j.1365-246X.2003.01919.x.